CWE-8
June 7-11, 2026
London, ON, Canada

Relationship between urban morphology and kinetic energy dissipation within urban area

Tazune Ito [a], Ryutaro Ogihara [b], Yasuyuki Ishida [c]

[a]*Tohoku University, Sendai, Japan, ito.tazune.q3@dc.tohoku.ac.jp*
[b]*Simizu Corporation, Tokyo, Japan, r.ogihara@shimz.co.jp*
[c] *Tohoku University, Sendai, Japan, yasuyuki.ishida.e1@tohoku.ac.jp*

SUMMARY

One method for improving urban ventilation involves promoting vertical air mixing within and above the urban canopy layer. However, enhancing vertical air mixing within a focused urban area accelerates the production and dissipation of turbulent kinetic energy, thereby reducing the kinetic energy available for improving the wind environment in leeward areas. To quantify the adverse effect, large-eddy simulations (LESs) were conducted for eight urban configurations with varying high-rise building heights and non-uniform building heights for the entire area. The results show that both the increased height of a high-rise building and the non-uniformity of building heights substantially enhanced the kinetic energy dissipation. Although some cases exhibited similar pedestrian-level wind speeds, the total kinetic energy dissipation differed significantly. These findings emphasize the need to assess the effects on the leeward side when urban morphology is changed to improve local wind environments.

Keywords: *Energy dissipation rate, High-rise building, Non-uniform building heights, LES, Breathability*

1. INTRODUCTION

Improving urban ventilation is an effective measure for heat adaptation within urban areas, and many studies have been conducted to investigate the relationship between urban morphology and wind velocity at pedestrian height (Ng et al., 2011; Carpentieri et al., 2015; etc.). However, even if the wind velocity is high, the environment cannot be considered favorable if the air is hot and polluted. From this perspective, Neophytou and Britter (2005) proposed the concept of "breathability," which analogizes urban ventilation to human breathing. This concept considers that outdoor urban spaces maintain cleanliness by "inhaling" fresh and cool air from areas where it is abundant, and "exhaling" hot and polluted air from outdoor spaces. Several researchers have evaluated breathability (Panagiotou et al., 2013; Chen et al., 2017; etc.). Most researchers regarded the upper urban atmosphere as a region of fresh and cool air and analyzed the enhancement of breathability by intensifying the air exchange between the upper and within-urban-canopy layers. A highly breathable condition implies that vertical air mixing is active through vertical advection and turbulent diffusion (Mochida et al., 2023), resulting in increased kinetic energy dissipation through the energy cascade mechanism. Consequently, areas located on the leeward side of highly breathable urban areas receive inflow air with reduced kinetic energy. Because of these considerations, evaluating the potential adverse effects on leeward areas in advance is essential when attempting to improve the wind environment of an urban area.

In one study in which adverse effects were evaluated, Ishida et al. (2018) analyzed the energy dissipation rate within a focused urban area and examined the implications for wind environments in leeward areas. Although kinetic energy dissipation depends on urban morphology, knowledge about this is scarce. Large-eddy simulations (LESs) were conducted in this study to quantify the influence of morphology on total kinetic energy dissipation for eight different morphology cases.

2. VALUATION INDICES USED IN THIS STUDY

The exact form of the energy dissipation rate of the total kinetic energy ε is defined by Eq. (1).

$$\varepsilon = 2\nu\langle\left\{\frac{1}{2}\left(\frac{\partial u_i}{\partial x_j}+\frac{\partial u_j}{\partial x_i}\right)\right\}^2\rangle = \nu\langle\frac{\partial u_i}{\partial x_j}\cdot\frac{\partial u_i}{\partial x_j}\rangle + \nu\frac{\partial^2\langle u_i u_j\rangle}{\partial x_i x_j} \quad (1)$$

where ν is kinetic viscosity, u_i and x_i are three components of the velocity vector and spatial coordinates (i = 1, 2, 3: streamwise, lateral, vertical), respectively, and $\langle f\rangle$ is the time-averaged value of a quantity f.

Following Ishida et al. (2018), the grid-scale energy dissipation rate ε_{GS} is calculated using Eq. (2), while the sub-grid-scale energy dissipation rate ε_{SGS} is obtained from the local equilibrium assumption, equating it to the production rate of sub-grid-scale kinetic energy P_{kSGS} as in Eq. (3).

$$\varepsilon_{GS} = \nu\langle\frac{\partial\bar{u}_i}{\partial x_j}\cdot\frac{\partial\bar{u}_i}{\partial x_j}\rangle = \nu\frac{\partial\langle\bar{u}_i\rangle}{\partial x_j}\cdot\frac{\partial\langle\bar{u}_i\rangle}{\partial x_j} + \nu\langle\frac{\partial\bar{u}'_i}{\partial x_j}\cdot\frac{\partial\bar{u}'_i}{\partial x_j}\rangle \quad (2)$$

$$\varepsilon_{SGS} = P_{kSGS} = -\langle\frac{\tau_{ij}}{\rho}\cdot\frac{\partial\bar{u}_i}{\partial x_j}\rangle \quad (3)$$

Here, $\langle\bar{f}\rangle$ is the filtered value of f, f' is the deviation from $\langle f\rangle$, and τ_{ij} is the SGS Reynolds stresses.

3. ANALYSIS OVERVIEW

LESs were conducted for urban areas with a high-rise building taller than its surroundings and non-uniform building heights in the entire urban area. The cases included eight types of staggered array of simplified building blocks with a plan area index of 25% (Figure 1 and Table 1). The inflow was generated using a method proposed by Okaze and Mochida (2017). A run-up calculation was performed over $t^* = 80$ [−] ($= t \times \langle u_{15H}\rangle/H$), and the turbulent statistics were collected and averaged over $t^* = 200$ [−]. Here, $\langle u_{15H}\rangle$ is the time-averaged wind velocity of the inflow at the boundary layer height ($15H$), and H is the building height in Case 1 (= 30 m). All quantities were normalized to H and $\langle u_{15H}\rangle$. Other conditions are listed in the NOTE at the end.

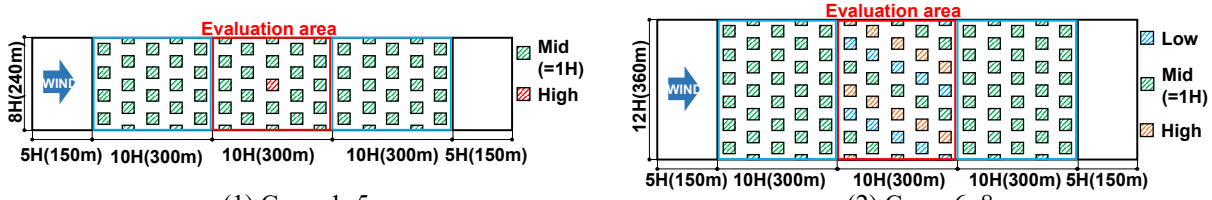

(1) Cases 1–5 (2) Cases 6–8

Figure 1: Computational domain and evaluation area (horizontal section).

Table 1: Total amount of kinetic energy dissipation.

Case	Building Height	σ/H_{ave}		Case	Building Height	σ/H_{ave}
Case 1	1H (uniform)	0		Case 5	1H and 7H (high-rise)	1.01
Case 2	1H and 2H (high-rise)	0.21		Case 6	0.75H, 1H, and 1.25H	0.20
Case 3	1H and 3H (high-rise)	0.40		Case 7	0.5H, 1H, and 1.5H	0.41
Case 4	1H and 5H (high-rise)	0.73		Case 8	0.25H, 1H, and 1.75H	0.61

4. RESULTS

In this abstract, the results for Case 1 (with uniform building height), Case 5 (with a single high-rise building), and Case 8 (with non-uniform height) are presented.

4.1. Mean Wind Velocity

Figures 2 and 3 present the spatial distribution of the mean wind velocity vectors in the vertical section at the domain center and in the horizontal section at pedestrian height (0.05H = 1.5 m), respectively. In Case 5, a strong downwind flow occurs on the windward side of the high-rise building (Figure 2b), increasing the wind velocity around the pedestrian spaces near the high-rise building (Figure 3b). In Case 8 (Figure 2c), however, non-uniformity disrupts the isolated flow observed around the buildings in Case 1 (uniform height, Figure 2a). At pedestrian level, the wind velocities generally increase around higher buildings (Figure 3c). The normalized spatially averaged values of the mean wind velocity in the evaluation area at pedestrian height are 0.143 in Case 1, and those for Cases 5 and 8 are 0.231 and 0.233, respectively, which are almost the same.

4.2. Turbulent Kinetic Energy

Figure 4 shows the vertical distribution of turbulent kinetic energy (TKE). In Case 1, TKE is generated up to approximately 2H. In Case 5, TKE increases significantly above and behind the high-rise building. In Case 8, the non-uniformity leads to higher TKE values than in Case 1, especially downstream of higher buildings, and the TKE, even within pedestrian spaces, increased.

4.3. Energy Dissipation Rate

Figure 5 shows vertical distributions of energy dissipation rates ε. Energy dissipation is high around roof level in Case 1, extending to about 2H. Dissipation is high around the high-rise building in Case 5. Downstream of the high-rise building, a wide high-dissipation region corresponds to the high-TKE region (Figure 4b). In Case 8, dissipation also occurs where TKE is high (Figure 4c).

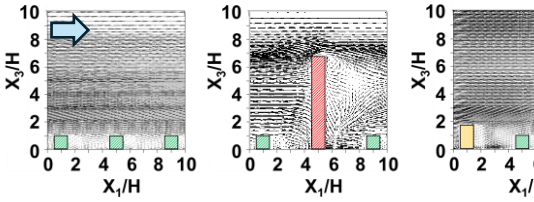

(a) Case 1 (b) Case 5 (c) Case 8

Figure 2: Wind velocity vector in vertical section.

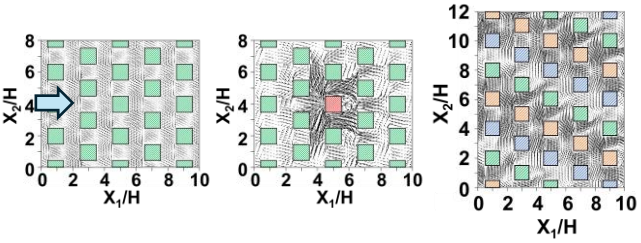

(a) Case 1 (b) Case 5 (c) Case 8

Figure 3: Wind velocity vector at pedestrian height.

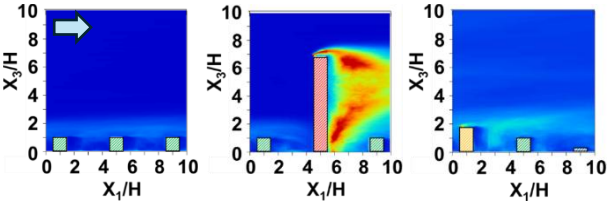

(a) Case 1 (b) Case 5 (c) Case 8

0 0.1 [-]

Figure 4: Turbulent kinetic energy in vertical section.

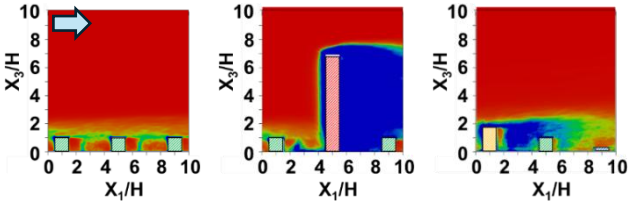

(a) Case 1 (b) Case 5 (c) Case 8

-0.001 0 [-]

Figure 5: Energy dissipation rate in vertical section.

Table 2 summarizes the total kinetic energy dissipation for each case. All cases show larger values than Case 1. Although Cases 5 and 8 have similar pedestrian-level mean wind speeds (Section 4.1), their total kinetic energy dissipations differ significantly. While Case 8 has 2.6 times the total kinetic energy dissipation of Case 1, Case 5 has over 8 times that of Case 1.

Table 2: Total amount of kinetic energy dissipation.

	Case 1	Case 2	Case 3	Case 4	Case 5	Case 6	Case 7	Case 8
ε_{total} [−]	−1.63	−2.17	−3.62	−8.18	−13.56	−3.02	−3.41	−4.23
$\varepsilon_{total}/\varepsilon_{total_{Case1}}$ [−]	1.00	1.33	2.22	5.02	8.32	1.85	2.09	2.60

5. CONCLUSION

The effects of the height of a high-rise building and the entire height non-uniformity in the examined urban area on the wind environment in leeward areas were analyzed based on total kinetic energy dissipation. Even when the pedestrian-level mean wind velocities are similar, the total kinetic energy dissipation, and hence the degree of adverse effects to the leeward areas, can vary substantially depending on the morphology of the urban area.

NOTE

Inflow profiles are shown in Figure 6. The code used is OpenFOAM-ver4.1. The grid system was a collocation grid. The time difference scheme was second-order implicit. The advection term scheme was a mixed scheme of 95% second-order central difference and 5% first-order upwind difference. The diffusion term scheme was second-order central difference. The pressure implicit with splitting of operators method was used for the pressure solution. The boundary condition of the top wall was slip, and that of the side wall was cyclic. Spalding law was used for the building wall and ground boundary condition. An advection-type condition was used for the outflow boundary.

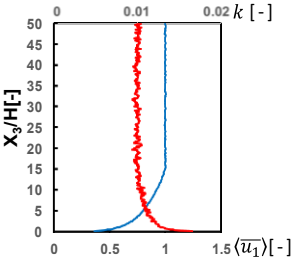

Figure 6: Inflow profiles.

ACKNOWLEDGEMENTS

This work was supported by JSPS KAKENHI Grant-in-Aid for Scientific Research (B), Grant Number JP23K26255. Part of the results were obtained using supercomputing resources at Cyberscience Center, Tohoku University.

REFERENCES

Carpentieri, M., Robins, A.G., 2015. Influence of urban morphology on air flow over building arrays, J. Wind Eng. Ind. Aerodyn. 145, 61–74. https://doi.org/10.1016/j.jweia.2015.06.001.

Chen, L., Hanga, J., Sandberg, M., Claesson, L., Sabatino, S. D., Wigo, H., 2017. The impacts of building height variations and building packing densities on flow adjustment and city breathability in idealized urban models, Building and Environment, 118, 344–361. https://doi.org/10.1016/j.buildenv.2017.03.042

Ishida Y., Okaze T., and Mochida A., 2018. Influence of urban configuration on the structure of kinetic energy transport and the energy dissipation rate, J. Wind Eng. Ind. Aerodyn. 183, 198–213. https://doi.org/10.1016/j.jweia.2018.10.016

Mochida, A., Ono, Y., Ishida, Y., Ogihara, R., 2023. Urban morphology promoting high breathability and controlling strong winds at the pedestrian level. Proceedings of 16th International Conference on Wind Engineering, 272.

Neophytou M.K.A., Britter R.E., 2005. Modelling of atmospheric dispersion in complex urban topographies: a computational fluid dynamics study of the central London area, 5th GRACM Int. Congr. Comput. Mech. 2, 9.

Ng, E., Yuan, C., Chen, L., Ren, C., Fung, J.C.H., 2011. Improving the wind environment in high-density cities by understanding urban morphology and surface roughness: A study in Hong Kong, Landsc. Urban Plan. 101, 59–74. https://doi.org/10.1016/j.landurbplan.2011.01.004.

Okaze T. and Mochida A, 2017.Cholesky decomposition–based generation of artificial inflow turbulence including scalar fluctuation, Computers & Fluids, 159, 23–32. https://doi.org/10.1016/j.compfluid.2017.09.005

Panagiotou, I., Neophytou, M.K.A., Hamlyn, D., Britter, R.E., 2013. City breathability as quantified by the exchange velocity and its spatial variation in real inhomogeneous urban geometries: An example from central London urban area, Science of the Total Environment, 442, 466–477. https://doi.org/10.1016/j.scitotenv.2012.09.001